PCCP

Accepted Manuscript

ROYAL SOCIETY OF CHEMISTRY

www.rsc.org/pccp

Journal Name

RSCPublishing

ARTICLE

Energetics and Efficiency Analysis of a Cobaloxime-Modified Semiconductor at Simulated Air Mass 1.5 Illumination

Cite this: DOI: 10.1039/x0xx00000x

Received 00th January 2012,
Accepted 00th January 2012

DOI: 10.1039/x0xx00000x

www.rsc.org/

Alexandra Krawicz,[a] Diana Cedeno[a] and Gary F. Moore[a]

We report on the energetics and efficiency of a p-type (100) gallium phosphide (GaP) semiconductor functionalized with molecular hydrogen production catalysts via polymer grafting. The catalysts belong to the cobaloxime class of compounds that have shown recent promise in electrocatalysis and solar-to-fuels applications. Attachment of the complex to a semiconductor surface allows direct photoelectrochemical (PEC) measurements of performance. Under simulated air mass 1.5 illumination, the catalyst-modified photocathode yields a 0.92 mA cm^{-2} current density when operating at the equilibrium potential for the hydrogen production half reaction. The open circuit photovoltage (V_{OC}) is 0.72 V vs. a reversible hydrogen electrode (RHE) and the fill factor (FF) is 0.33 (a 258% increase compared to polymer-modified electrodes, without cobaloxime treatment). The external quantum efficiency (EQE), measured under a reverse bias of +0.17 vs. RHE, shows a maximum of 67% under 310 nm illumination. Product analysis of the head-space gas yields a lower limit on the Faradaic efficiency of 88%. In addition, the near linear photoresponse of the current density upon increasing illumination indicates that photocarrier transport to the interface can limit performance. These results give insights to designing improved photocatalytic constructs with additional performance gains.

Introduction

Artificial photosynthesis is a long-sought goal in solar energy research.[1-3] By splitting water into oxygen and a source of reducing equivalents (protons and electrons) for producing a fuel, two problems are addressed: energy storage and the production of a potential carbon-neutral transport fuel.[4-7] However, effective strategies to interface light capture and conversion technologies with emerging catalysts for energy storage remain an outstanding scientific challenge.[8, 9] In biology, enzymes catalyze a myriad of technologically relevant chemical reactions by providing discrete three-dimensional environments (molecular catalysts) for binding substrates, releasing products, and lowering transition-state energies along a reaction coordinate.[10, 11] Thus, in accordance with the Sabatier principle, they can have exceptionally high activities and, perhaps more impressively, selectivity for specific chemical transformations. However, not every aspect of biology should necessarily be a target of chemical mimicry.[12] For example, in photosynthesis the efficiency of the initial light capture and charge separation steps is near unity, but losses due to inherited metabolic processes and use of intermediate energy carriers reduce the overall energy conversion efficiency to less than a few percent.[13, 14]

In principle, human-engineered systems could bypass such constraints by having fewer energy transduction steps with improved interfaces. This will require strategies to engineer bulk materials and surfaces with enhanced electronic quality, stability and catalytic functionality.[15-19] Currently, a majority of molecular fuel catalysts are initially designed and optimized for operation in solution, with the use of external chemical agents or an electrode providing the driving force.[20-25] Thus, it is often uncertain how or if a given complex will function when immobilized on a conductive electrode or semiconductor surface. Conversely, understandings of the properties that promote favorable photocatalytic function are hampered by a lack of functional systems and subsystems.

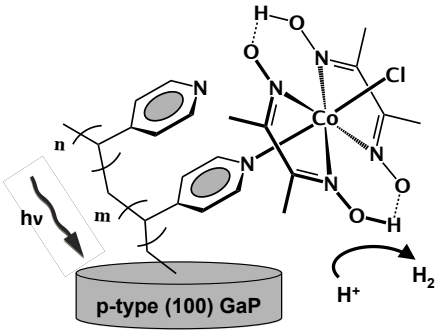

Figure 1. Schematic depiction of a cobaloxime-modified GaP semiconductor. Illumination of the hybrid construct with visible light generates a photovoltage that drives hydrogen production at the cobaloxime-modified surface.

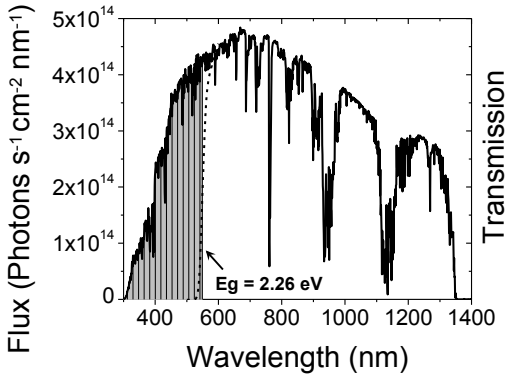

Figure 2. The air mass 1.5 global tilt solar flux spectrum (solid) and the transmission spectrum of the GaP substrates used in these experiments (dashed). The shaded grey area shows the integrated region of the solar spectrum from 280 nm up to the band gap of GaP (Eg = 2.26 eV = 549 nm), representing the theoretical maximum number of photons ($6.0x10^{16}$ photons s^{-1} cm^{-2}) that can be collected.

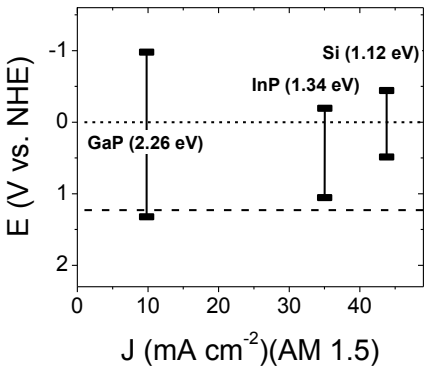

Figure 3. Conduction band (top bar) and valance band (bottom bar) positions vs. NHE of GaP (Eg = 2.26 eV), InP (Eg = 1.34 eV) and Si (1.12 eV). The abscissa indicates the maximum theoretical photocurrent under air mass 1.5 illumination. The dotted and dashed lines indicate the reversible potential of the H^+/H_2 and O_2/H_2O half reactions, respectively.

Nonetheless, the development of advanced materials and techniques for manipulating matter on the nanoscale has allowed significant advances toward mimicking favorable aspects of the chemistry of biological systems into human-engineered constructs.[15-43]

We have recently reported a modular approach to interfacing visible-light absorbing semiconductors, including p-type (100) GaP and p-type (111) Si, with fuel production catalysts.[40] The grafting procedure exploits the UV-induced immobilization chemistry of alkenes to a semiconductor surface,[44-50] providing a means for attaching molecular catalytic complexes to surface bound linkers. The modular aspect of this method allows independent modification of the light absorber, bridging material, anchoring functionality, or catalysts as new materials and discoveries emerge. In addition, we have also reported a photofunctional construct composed of molecular cobalt-containing hydrogen production catalysts interfaced to a polyvinyl-pyridine-modified GaP surface (Co-PVP-GaP) (Fig. 1).[36] The catalysts belong to the cobaloxime class of compounds that have shown recent promise in electrocatalysis, both in solution and immobilized at conductive substrates as well as solar-to-fuels applications in systems using molecular sensitizers, wide-band gap semiconductors or biological photosytems.[27-34]

In the assembly reported here, catalyst attachment to a polymer-modified semiconductor (PVP-GaP) allows direct measurement of photoelectrochemical performance. Co-PVP-GaP catalyzes what is otherwise a sluggish reaction, requiring relatively large overpotentials to achieve similar rates when using electrodes without cobaloxime treatment. For example, in a previous report[36] we show that a Co-PVP-GaP electrode under 100 mW cm^{-2} illumination using a Newport Oriel Apex illuminator source yields a 2.4 mA cm^{-2} current density when poised at a potential 310 mV below the equilibrium potential of the H^+/H_2 redox couple. To achieve a similar photocurrent density using a PVP-GaP working electrode (without catalyst treatment), a 270 mV overpotential must be applied. The production of current at an underpotential indicates that only light, and no external electrochemical forward biasing, is required to generate the photocurrent and associated hydrogen. In addition, the Co-functionalized material shows an increased stability as compared to bare GaP (a >175% increase), as evidenced by the percent decrease in photocurrent over time in Co-PVP-GaP versus GaP (without cobaloxime-polymer modification). Herein, we report a more detailed energetics and efficiency analysis of these constructs including photovoltaic parameters, quantum efficiency and Faradaic efficiency obtained using modified- and unmodified- GaP substrates at selected illumination conditions and applied bias potentials.

Results and discussion

Component Optical and Electronic Properties. GaP is a midsize optical band gap (indirect Eg = 2.26 eV) semiconductor with a conduction band (CB) edge poised ~ 1 V negative of the hydrogen production half reaction. Thus, in addition to commercial importance in light emitting diode technologies, GaP is a promising candidate material for applications in solar-fuel generator technologies.[51-57] Although, the band gap of this material limits the fraction of total solar photons available for absorption, the energetic positioning of GaP's CB is an attractive feature for investigation of interfaces to fuel production catalysts that may require significant overpotentials.

The transmission spectra of the GaP wafer used in this study as well as the air mass 1.5 global tilt (AM 1.5G) solar spectrum[58] are shown in Figure 2. The conduction band and valence band positions of GaP as well as the theoretical maximum photocurrent density set by its optical properties are shown in Figure 3. Information on other p-type semiconductors (InP and Si) is included for comparison. Integration of the AM 1.5G solar spectrum up to the GaP absorption threshold yields a photon flux of $6.0x10^{16}$ photons s^{-1} m^{-2}. If all available photons give rise to current, the maximum theoretical photocurrent density is 9.6 mA cm^{-2}. However, actual photocurrent densities are always lower given reflection and transmission losses (Fig. 4) as well as other "parasitic" processes[59] that preclude absorbed photons from being converted to charge carriers moving through a potential. In addition, catalysts immobilized at a surface can also absorb a fraction of the incident photons.[60] An absorption spectrum of a model cobaloxime catalyst, $Co(dmgH)_2PyCl$, recorded

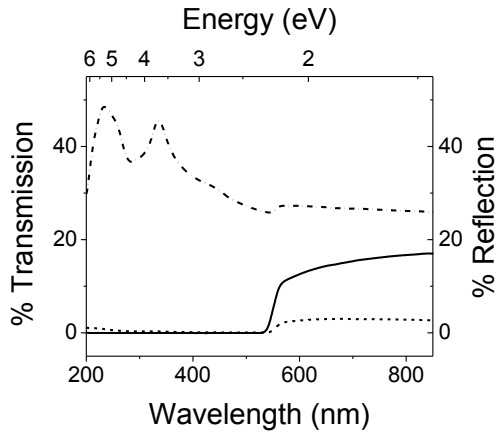

Figure 4. The transmission spectrum (solid) as well as the relative specular (dash-dot) and diffuse (dashed) reflectance spectra of the GaP substrates used in these experiments.

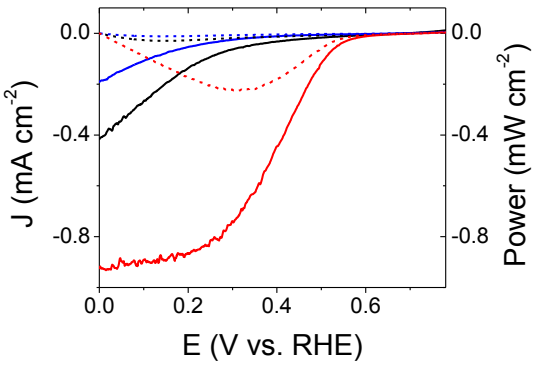

Figure 5. Linear sweep voltammograms (solid lines) and associated power curves (dashed lines) of GaP (black) PVP-GaP (blue) and Co-PVP-GaP (red) working electrodes at pH 7 under 100 mW cm^{-2} illumination using a Solar Light PV Cell Test Simulator.

as an acetonitrile solution is shown in Figure S1. The complex shows characteristic absorption features of the Co^{III} complex[28] including high-energy absorption bands with λ_{max} at 223 nm and 253 nm corresponding to spin-allowed intraligand (π-π*) transitions.

The p-type character of the modified-semiconductor electrodes used in these experiments precludes analysis of the constructs as a dark electrocatalyst. A cyclic voltammogram of the model compound $Co(dmgH)_2PyCl$ (Fig. S2) recorded in a 0.1 M $TBAPF_6$ acetonitrile solution at a glassy carbon working electrode shows a chemically irreversible redox process with E_p = -0.98 V vs. Fc/Fc^+ (-0.34 V vs. NHE),[61] assigned to the Co^{III}/Co^{II} redox couple, and a chemically reversible redox process with $E_{1/2}$ = -1.46 V vs. Fc/Fc^+ (-0.82 V vs. NHE), assigned to the Co^{II}/Co^{I} relay. These peak positions are consistent with previous reports on this complex[28] and give an approximation of the photovoltages required to access these couples during catalytic operation. However, values obtained using a homogenous complex in organic solvents may be significantly different from those of analogous surface immobilized species (i.e. heterogenized-homogenous catalysts) in aqueous environments. For example, reports of a structurally similar cobaloxime catalyst immobilized on dye-sensitized TiO_2 nanoparticles giving rise to photoinduced hydrogen production in an aqueous environment indicate the Co^{II}/Co^{I} couple is positive of the TiO_2 conduction band under the reported experimental conditions.[32] Nonetheless, in the experiments reported here the relatively negative potential of the GaP conduction band should ensure thermodynamically favorable conditions for photoactivating attached cobaloxime complexes.

Construct Photoelectrochemical Properties. Three-electrode current density-voltage (J-V) responses and associated power curves of a cobaloxime-modified electrode at simulated AM 1.5 solar illumination are shown in Figure 5. The GaP substrates used in these experiments are Zn doped with a resistivity of 5.5×10^{-2} Ω·cm, a mobility of 54 $cm^2\ V^{-1}s^{-1}$ and a carrier concentration of 2.2×10^{18} cm^{-3}. Co-PVP-GaP working electrodes show significant improvement in photoperformance compared to electrodes without catalyst modification. Under simulated AM 1.5 illumination, Co-PVP-GaP yields a 0.92 mA cm^{-2} current density when operating at the equilibrium potential for the hydrogen production half reaction. For comparison, electrodes without cobalt treatment show a 0.42 mA cm^{-2} and 0.19 mA cm^{-2} current density for GaP and PVP-GaP respectively. In these experiments, under simulated AM1.5 illumination, the open circuit potential (V_{OC}) for the GaP, PVP-GaP, and Co-PVP-GaP electrodes is 0.69 V, 0.68 V, and 0.72 V vs. RHE respectively. Comparison of the V_{OC} values obtained for PVP-GaP and Co-PVP-GaP photoelectrodes reveals a positive shift that is indicative of increased catalytic activity following incorporation of the Co catalyst. The fill factor (FF), defined as the maximum power output divided by the product of the Voc and the short-circuit current density (J_{SC}) with respect to the desired half reaction, improves dramatically for the Co catalyst functionalized electrodes. The fill factor, of the Co-PVP-GaP electrode is 0.33 (a 119% and 258% increase as compared to GaP and PVP-GaP respectively). Due to the steep increase in operating photocurrent densities that are produced by small changes in the FF of a photocathode and/or photoanode, even small changes in FF can have a significant effect on the solar-to-hydrogen efficiencies of a complete two-electrode assembly.

The J-V response of PVP-GaP and Co-PVP-GaP upon increasing illumination intensity is shown in Figure 6. For the Co-PVP-GaP electrode, increasing illumination intensity results in relatively little change of the V_{OC} or FF. However, the J_{SC} increases approximately linearly with illumination intensity (Fig. 7), indicating that photocarrier transport to the interface can limit the performance of the Co-modified GaP photocathodes. A similar trend is observed for PVP-GaP, albeit at overall lower photocurrent densities (Fig. S3). As reported in a previous publication,[36] even higher current densities can be obtained for Co-PVP-GaP, reaching 2.4 mA cm^{-2} at a 310 mV underpotential, when using a Xenon lamp illumination source without an AM 1.5 filter and after optimizing the doping of the GaP wafers (Fig. S4 & Fig. S5).

Photocurrents were also measured under monochromatic light at selected potentials. External quantum efficiencies were calculated using the measured values of the photocurrents and the intensity of the illumination source. The spectral response of the external quantum efficiency (EQE) of PVP-GaP and Co-PVP-GaP electrodes

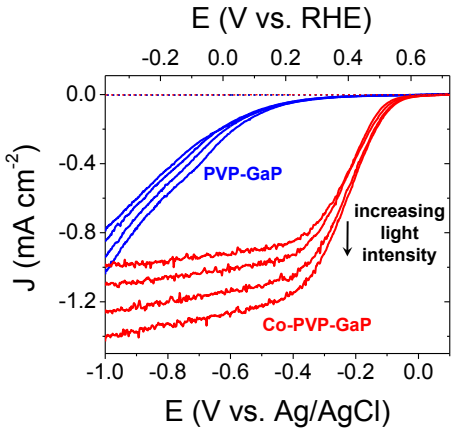

Figure 6. Linear sweep voltammograms of PVP-GaP (blue) and Co-PVP-GaP (red) working electrodes at pH 7 in the dark (dashed lines) and with illumination (solid lines) at 100 mW cm^{-2}, 120 mW cm^{-2}, 135 mW cm^{-2}, and 150 mW cm^{-2}.

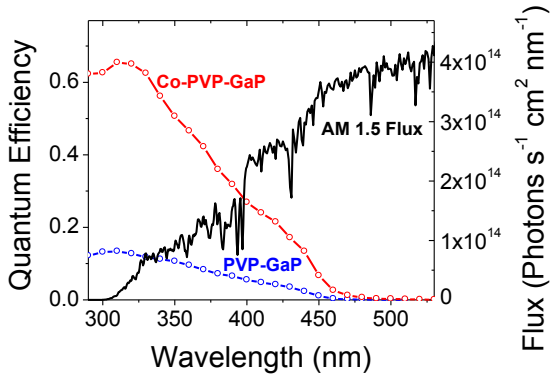

Figure 8. External quantum efficiency of PVP-GaP (blue) and Co-PVP-GaP (red) working electrodes poised at +0.17 V vs. RHE and the air mass 1.5 global tilt solar flux spectrum at wavelengths that are actinically relevant to GaP.

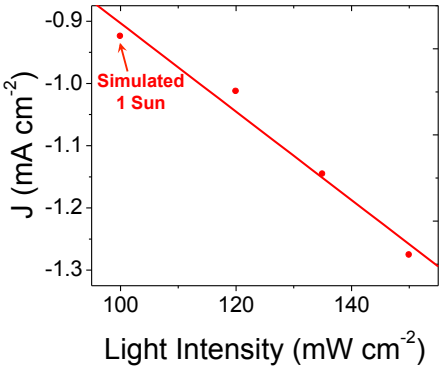

Figure 7. Photocurrent density (at 0.00 V vs. RHE) of a Co-PVP-GaP electrode recorded at increasing illumination (data points are taken from the plots shown in Figure 6).

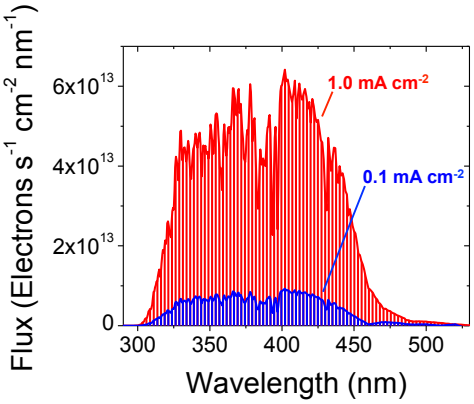

Figure 9. Calculated electron flux of the PVP-GaP (blue) Co-PVP-GaP (red) electrode at AM 1.5 illumination.

poised at +0.17 V vs. RHE are shown in Figure 8. A measurable photocurrent is observed at wavelengths lower than ~550 nm, consistent with the GaP indirect band gap. Likewise, the sharp rise in photocurrent at wavelengths lower than ~ 450 nm is characteristic of the GaP direct band gap (2.8 eV). Using the QE data, the calculated electron flux (i.e. current) produced by PVP-GaP and Co-PVP-GaP samples poised at +0.17 V vs. RHE under AM 1.5G illumination is shown in Figure 9. Integration of the spectra yields current densities of 8.9×10^{14} electrons s^{-1} cm^{-2} = 0.1 mA cm^{-2} and 6.4×10^{15} electrons s^{-1} cm^{-2} s^{-1} = 1.0 mA cm^{-2}, for PVP-GaP and Co-PVP-GaP respectively, indicating that the solar simulator used in the J-V measurements closely approximates AM 1.5G conditions. Comparison of the AM 1.5G solar flux, integrated over 280-4000 nm ($4.3\text{x}10^{17}$ photons s^{-1} cm^{-2}), with the Co-PVP-GaP electron flux, shown in Figure 9 yields an overall EQE of 1.5%. Considering only photons in the GaP actinic range, from 280-549 nm (Fig. 1), the EQE is 11%.

Confirmation of hydrogen production and a measure of the Faradaic efficiency was performed via analysis of the head-space gas using a gas chromatograph equipped with a thermal conductivity detector (see Methods section). Following 30 minutes of simulated AM 1.5 illumination of a Co-PVP-GaP electrode poised at +0.17 V vs. RHE, a lower limit on the Faradaic efficiency of 88% was determined.

Experimental

Materials and Methods. Single crystalline (100) GaP wafers were purchased from ITME Warsaw, Poland. The wafers were Zn doped *p*-type with a resistivity of 5.5×10^{-2} Ω·cm, a mobility of 54 cm^2 $V^{-1}s^{-1}$ and a carrier concentration of 2.2×10^{18} cm^{-3}. The etch pit density (EPD) was 3.7×10^4 cm^{-2}. The wafers used for the Faradaic efficiency measurement were also from ITME with a resistivity of 2.93×10^{-1} Ω·cm, a mobility of 70 cm^2 $V^{-1}s^{-1}$, carrier concentration of 3.05×10^{17} cm^{-3} and etch pit density (EPD) of 5.7×10^4 cm^{-2} . The material was single side polished to an epi-ready finish. Diced semiconductor samples were degreased by wiping the surface with an acetone soaked cotton swab, and sonication in acetone and

isopropanol, followed by drying under flowing nitrogen. Samples were then exposed to an air-generated oxygen plasma (Harrick Plasma, USA) at 30 W for 2 min. Surface oxide layers were then removed in a glove box by immersion of the plasma-treated samples in buffered hydrofluoric acid (6:1 HF:NH_4F in H_2O) for 5 min, followed by rinsing with anhydrous methanol and drying under vacuum. All synthesis was carried out under an argon atmosphere using Schlenk techniques or in a nitrogen glove box. All reagents were purchased from Aldrich. All solvents were stored over the appropriate molecular sieves prior to use. MilliQ water (18.2 MΩ·cm) was used to prepare all aqueous solutions. The cobaloxime catalyst precursor, $Co(dmgH_2)(dmgH)Cl_2$, and the cobaloxime catalyst, $Co(dmgH)_2PyCl$, were prepared according to a previously reported procedure.[62,63]

Preparation of polyvinylpyridine-grafted GaP. Freshly cleaned and etched (see Materials section) (100) GaP wafers were placed in a quartz flask and covered with inhibitor-free 4-vinylpyridine. The flask was illuminated with UV light (254nm, SPECTROLINE(R) E-SERIES UV LAMP) for 2 h with the polished surface of GaP facing the light source. The modified wafers were then washed with copious amounts anhydrous methanol before drying under vacuum.

Preparation of cobaloxime-modified GaP. PVP-grafted wafers of (100) GaP were dipped in a solution of $Co(dmgH_2)(dmgH)Cl_2$ (1 mM in methanol) in the presence of triethylamine (1 mM in methanol) overnight. The modified wafers were rinsed with anhydrous methanol and isopropanol (99%) before drying under nitrogen.

Preparation of working electrodes. Wafers were sonicated in isopropanol (99%). GaP working electrodes were fabricated by applying an indium-gallium eutectic (Aldrich) to the backside of a wafer, then fixing a copper wire to the back of the wafer using a conductive silver epoxy (Circuit Works). The copper wire was passed through a glass tube and the wafer was insulated and attached to the glass tube with Loctite 615 Hysol Epoxi-patch adhesive. The epoxy was allowed to dry overnight before testing the electrodes.

Instrumentation and Experimental Details.

UV-vis. Ultraviolet-visible (UV-vis) optical spectra were recorded on a Shimadzu SolidSpec-3700 spectrometer with a deuterium lamp for the ultraviolet range and a tungsten (halogen) lamp for the visible and near infrared. Transmission and reflectance measurements were performed with an integrating sphere.

NMR. Nuclear magnetic resonance (NMR) spectra were recorded on a Bruker 500'54 Ascend spectrometer operating at 500 MHz. Unless otherwise stated, all spectra were collected at room temperature.

Electrochemistry. Cyclic voltammetry was performed with a Biologic potentiostat using a glassy carbon (3 mm diameter) disc, a platinum counter electrode, and a silver wire pseudoreference electrode in a conventional three-electrode cell. Anhydrous acetonitrile (Aldrich) was used as the solvent for electrochemical measurements. The supporting electrolyte was 0.10 M tetrabutylammonium hexafluorophosphate. The solution was deoxygenated by bubbling with argon. The working electrode was cleaned between experiments by polishing with alumina (50 nm dia.) slurry, followed by solvent rinses. The potential of the pseudoreference electrode was determined using the ferrocenium/ferrocene redox couple as an internal standard (with $E_{1/2}$ taken as 0.40 V vs. NHE). The voltammograms were recorded at sweep rates of 100 mV s^{-1}. Linear sweep voltammetry and three-electrode electrolysis (chronoamperometry) were performed with a Biologic potentiostat using a platinum counter electrode, a Ag/AgCl, NaCl (3 M) reference electrode (0.21 V vs. NHE), and GaP working electrodes (including: GaP following buffered HF treatment, PVP-GaP and Co-PVP-GaP) in a modified cell containing a quartz window. The supporting electrolyte was 0.1 M phosphate buffer (pH = 7). Measurements were performed under a continuous flow of 5% hydrogen in nitrogen. Photoelectrochemical (PEC) testing was performed using a Solar Light PV Cell Test Simulator model 16S-300-005V4.0 Xenon lamp with an AM 1.5 filter and a XPS-300 power supply at 100 mW cm^{-2} illumination. All data were recorded following initial light dark testing.

Quantum Efficiency Measurements. Incident photon to current efficiency (IPCE) was measured at a bias of +0.17 V vs. RHE in the wavelength range relevant to GaP's band gap. The experimental setup consisted of a NIST calibrated silicon photodiode FDS100 to calibrate the light intensity, an Oriel Xenon 150W lamp with a Newport 69907 power supply, an Oriel Cornerstone 130 1/8m monochromator, a 200/1mm grating (slit width was 2mm for a resolution of 0.5nm), a Gamry Instruments Reference 600 potentiostat/galvanostat ZRA and a Keithley 2400 Source Meter.

Faradaic Efficiency Measurements. Hydrogen was detected via gas chromatography (GC) using a micro GC (Agilent 490). A Co-PVP-GaP electrode was placed in a glass electrochemical cell with a quartz window and purged with argon for 30 min before sealing the vessel. Argon (15mL) was withdrawn from the cell with a syringe and replaced with an equivalent volume of methane (99%) analytical internal standard (Aldrich). The potential was then set to +0.17 V vs. RHE and held at that value for 30 min to accumulate the product. An aliquot of the headspace gas was withdrawn with a syringe and injected into the GC.

Conclusions

Under simulated AM 1.5 illumination, Co-PVP-GaP yields a 0.9 mA photocurrent density when poised at a potential 170 mV below the equilibrium potential of the H^+/H_2 redox couple. These results indicate only light, and no external electrochemical forward biasing is required to generate the photocurrent. For PVP-GaP, the lack of active catalytic sites results in a greater probability of minority carrier recombination at the interface. Therefore, a more negative applied potential, which increases the surface band bending and suppresses charge carrier recombination, is required to achieve a given photocurrent density.

The EQE of Co-PVP-GaP, measured at +0.17 vs. RHE, shows a maximum of 67% under 310 nm illumination. However, the band gap of GaP (2.26 eV) significantly limits the total number of solar photons that can be collected and the overall EQE (1.5%). The J-V response upon increasing illumination indicates that photocarrier transport to the interface can limit the performance of Co-PVP-GaP at simulated AM 1.5 illumination, indicating that additional performance gains may be obtained by using semiconductors with improved spectral coverage of the solar spectrum. Of course use of such light

absorbers may require incorporation of catalysts capable of operating with relatively lower potential requirements.

The work reported here illustrates the potential to directly couple human-engineered catalysts for fuel production with light capture and conversion materials. The modular aspect of our assembly method should allow researchers to use and adapt this chemistry as new materials and discoveries emerge. This approach could allow catalysts made from earth-abundant elements, tethered over photocathodes, to replace the use of precious metal catalysts currently implemented in many solar-fuel generator prototypes as well as other technologies capable of reducing net carbon dioxide emissions.

Acknowledgements

This material is based upon work performed by the Joint Center for Artificial Photosynthesis, a DOE Energy Innovation Hub, supported through the Office of Science of the U.S. Department of Energy under Award Number DE-SC0004993. The authors thank Mark Hettick for assistance with the IPCE measurements, as well as valuable discussions and comments regarding the manuscript.

Notes and references

[a] Joint Center for Artificial Photosynthesis (JCAP), Lawrence Berkeley National Laboratory, Berkeley, California 94720, USA.

Electronic Supplementary Information (ESI) available: [electrochemical and photoelectrochemical data, lamp spectra, NMR]. See DOI: 10.1039/b000000x/

1. A. J. Bard and M. A. Fox, *Acc. Chem. Res.*, 1995, **28**, 141-145.
2. G. Ciamician, *Science*, 1912, **36**, 385-394.
3. M. S. Wrighton, *Science*, 1986, **231**, 32-37.
4. H. B. Gray, *Nat. Chem.*, 2009, **1**, 7-7.
5. N. S. Lewis and D. G. Nocera, *Proc. Natl. Acad. Sci.*, 2006, **103**, 15729-15735.
6. T. Faunce, S. Styring, M. R. Wasielewski, G. W. Brudvig, A. W. Rutherford, J. Messinger, A. F. Lee, C. L. Hill, H. deGroot, M. Fontecave, D. R. MacFarlane, B. Hankamer, D. G. Nocera, D. M. Tiede, H. Dau, W. Hillier, L. Wang and R. Amal, *Energy Environ. Sci.*, 2013, **6**, 1074-1076.
7. T. A. Faunce, W. Lubitz, A. W. Rutherford, D. MacFarlane, G. F. Moore, P. Yang, D. G. Nocera, T. A. Moore, D. H. Gregory, S. Fukuzumi, K. B. Yoon, F. A. Armstrong, M. R. Wasielewski and S. Styring, *Energy Environ. Sci.*, 2013, **6**, 695-698.
8. *Directing Matter and Energy: Five Challenges for Science and the Imagination*, U.S. Dept. of Energy, Washington, D. C., December, 2007.
9. *New Sciences for a Secure and Sustainable Energy Future*, U.S. Dept. of Energy, Wahshington, D.C., December, 2008.
10. W. J. Albery and J. R. Knowles, *Biochemistry*, 1976, **15**, 5631-5640.
11. F. A. Armstrong and J. Hirst, *Proc. Natl. Acad. Sci.*, 2011, **108**, 14049-14054.
12. A. W. Rutherford and T. A. Moore, *Nature*, 2008, **453**, 449-449.
13. R. E. Blankenship, D. M. Tiede, J. Barber, G. W. Brudvig, G. Fleming, M. Ghirardi, M. R. Gunner, W. Junge, D. M. Kramer, A. Melis, T. A. Moore, C. C. Moser, D. G. Nocera, A. J. Nozik, D. R. Ort, W. W. Parson, R. C. Prince and R. T. Sayre, *Science*, 2011, **332**, 805-809.
14. L. Hammarström, J. R. Winkler, H. B. Gray and S. Styring, *Science*, 2011, **333**, 288.
15. G. F. Moore and G. W. Brudvig, *Annu. Rev. Condens. Matter Phys.*, 2011, **2**, 303-327.
16. M. M. Najafpour, J.-R. Shen, J. Barber, G. F. Moore and Govindjee, *Chem. World*, 2012, **43**.
17. J. R. Swierk and T. E. Mallouk, *Chem. Soc. Rev.*, 2013, **42**, 2357-2387.
18. P. D. Tran, L. H. Wong, J. Barber and J. S. C. Loo, *Energy Environ. Sci.*, 2012, **5**, 5902-5918.
19. M. G. Walter, E. L. Warren, J. R. McKone, S. W. Boettcher, Q. Mi, E. A. Santori and N. S. Lewis, *Chem. Rev.*, 2010, **110**, 6446-6473.
20. V. Artero and M. Fontecave, *Coord. Chem. Rev.*, 2005, **249**, 1518-1535.
21. Z. Han, F. Qiu, R. Eisenberg, P. L. Holland and T. D. Krauss, *Science*, 2012, **338**, 1321-1324.
22. Z. Han, L. Shen, W. W. Brennessel, P. L. Holland and R. Eisenberg, *J. Am. Chem. Soc.*, 2013, **135**, 14659-14669.
23. M. L. Helm, M. P. Stewart, R. M. Bullock, M. R. DuBois and D. L. DuBois, *Science*, 2011, **333**, 863-866.
24. S. Losse, J. G. Vos and S. Rau, *Coord. Chem. Rev.*, 2010, **254**, 2492-2504.
25. K. L. Mulfort, A. Mukherjee, O. Kokhan, P. Du and D. M. Tiede, *Chem. Soc. Rev.*, 2013, **42**, 2215-2227.
26. R. Brimblecombe, A. Koo, G. C. Dismukes, G. F. Swiegers and L. Spiccia, *J. Am. Chem. Soc.*, 2010, **132**, 2892-2894.
27. V. Artero, M. Chavarot-Kerlidou and M. Fontecave, *Angew. Chem. Int. Ed.*, 2011, **50**, 7238-7266.
28. J. L. Dempsey, B. S. Brunschwig, J. R. Winkler and H. B. Gray, *Acc. Chem. Res.*, 2009, **42**, 1995-2004.
29. J. Huang, K. L. Mulfort, P. Du and L. X. Chen, *J. Am. Chem. Soc.*, 2012, **134**, 16472-16475.
30. Z. Ji, M. He, Z. Huang, U. Ozkan and Y. Wu, *J. Am. Chem. Soc.*, 2013, **135**, 11696-11699.
31. F. Lakadamyali and E. Reisner, *Chem. Commun.*, 2011, **47**, 1695-1697.
32. A. Reynal, F. Lakadamyali, M. A. Gross, E. Reisner and J. R. Durrant, *Energy Environ. Sci.*, 2013, **6**, 3291-3300.
33. L. M. Utschig, S. C. Silver, K. L. Mulfort and D. M. Tiede, *J. Am. Chem. Soc.*, 2011, **133**, 16334-16337.
34. B. S. Veldkamp, W.-S. Han, S. M. Dyar, S. W. Eaton, M. A. Ratner and M. R. Wasielewski, *Energy Environ. Sci.*, 2013, **6**, 1917-1928.
35. J. M. Gardner, M. Beyler, M. Karnahl, S. Tschierlei, S. Ott and L. Hammarström, *J. Am. Chem. Soc.*, 2012, **134**, 19322-19325.
36. A. Krawicz, J. Yang, E. Anzenberg, J. Yano, I. D. Sharp and G. F. Moore, *J. Am. Chem. Soc.*, 2013, **135**, 11861-11868.
37. G. Li, E. M. Sproviero, W. R. McNamara, R. C. Snoeberger, R. H. Crabtree, G. W. Brudvig and V. S. Batista, *J. Phys. Chem. B*, 2009, **114**, 14214-14222.
38. L. Li, L. Duan, Y. Xu, M. Gorlov, A. Hagfeldt and L. Sun, *Chem. Commun.*, 2010, **46**, 7307-7309.
39. G. F. Moore, J. D. Blakemore, R. L. Milot, J. F. Hull, H.-e. Song, L. Cai, C. A. Schmuttenmaer, R. H. Crabtree and G. W. Brudvig, *Energy Environ. Sci.*, 2011, **4**, 2389-2392.

40. G. F. Moore and I. D. Sharp, *J. Phys. Chem. Lett.*, 2013, **4**, 568-572.
41. W. Song, C. R. K. Glasson, H. Luo, K. Hanson, M. K. Brennaman, J. J. Concepcion and T. J. Meyer, *J. Phys. Chem. Lett.*, 2011, **2**, 1808-1813.
42. W. J. Youngblood, S.-H. A. Lee, Y. Kobayashi, E. A. Hernandez-Pagan, P. G. Hoertz, T. A. Moore, A. L. Moore, D. Gust and T. E. Mallouk, *J. Am. Chem. Soc.*, 2009, **131**, 926-927.
43. Y. Zhao, J. R. Swierk, J. D. Megiatto, B. Sherman, W. J. Youngblood, D. Qin, D. M. Lentz, A. L. Moore, T. A. Moore, D. Gust and T. E. Mallouk, *Proc. Natl. Acad. Sci.*, 2012.
44. J. M. Buriak, *Chem. Rev.*, 2002, **102**, 1271-1308.
45. T. Chen, I. Amin and R. Jordan, *Chem. Soc. Rev.*, 2012, **41**, 3280-3296.
46. R. L. Cicero, M. R. Linford and C. E. D. Chidsey, *Langmuir*, 2000, **16**, 5688-5695.
47. D. Richards, D. Zemlyanov and A. Ivanisevic, *Langmuir*, 2010, **26**, 8141-8146.
48. T. B. Stachowiak, F. Svec and J. M. J. Fréchet, *Chem. Mater.*, 2006, **18**, 5950-5957.
49. M. Steenackers, A. Ku□ller, S. Stoycheva, M. Grunze and R. Jordan, *Langmuir*, 2009, **25**, 2225-2231.
50. X. Wang, R. E. Ruther, J. A. Streifer and R. J. Hamers, *J. Am. Chem. Soc.*, 2010, **132**, 4048-4049.
51. E. E. Barton, D. M. Rampulla and A. B. Bocarsly, *J. Am. Chem. Soc.*, 2008, **130**, 6342-6344.
52. J. O. M. Bockris and K. Uosaki, *J. Electrochem. Soc.*, 1977, **124**, 1348-1355.
53. M. Gratzel, *Nature*, 2001, **414**, 338-344.
54. B. Kaiser, D. Fertig, J. Ziegler, J. Klett, S. Hoch and W. Jaegermann, *Chem. Phys. Chem.*, 2012, **13**, 3053-3060.
55. J. Sun, C. Liu and P. Yang, *J. Am. Chem. Soc.*, 2011, **133**, 19306-19309.
56. Y. Sun, J. Sun, J. R. Long, P. Yang and C. J. Chang, *Chem. Sci.*, 2013, **4**, 118-124.
57. M. Tomkiewicz and J. M. Woodall, *Science*, 1977, **196**, 990-991.
58. At the time of writing, the air-mass 1.5 global tilt (AM 1.5G) solar spectrum, from the ASTM G173-03 data set, is available online at http://rredc.nrel.gov/solar/spectra/am1.5/
59. W. Shockley and H. J. Queisser, J. *Appl. Phys.,* 1961, 3**2,** 510-519.
60. L. Trotochaud, T. J. Mills and S. W. Boettcher, J. *Phys. Chem. Lett.,* 2013, 4**,** 931-935.
61. All redox potentials were measured relative to ferrocenium/ferrocene (Fc+/Fc). To facilitate comparison with previous reports on the electochemistry of Co(dmgH)2PyCl, the Fc+/Fc couple is taken as (0.40 V vs SCE) then adjusted to NHE (SCE vs NHE = 0.24 V). We advise caution in directly comparing literature values reported in V vs. NHE as conversion factors from the actual reference electrode used in the experiment and experimental conditions are not always consistent.
62. W. C. Trogler, R. C. Stewart, L. A. Epps and L. G. Marzilli, I*norg. Chem.,* 1974, 1**3,** 1564-1570.
63. dmgH = dimethylglyoximate monoanion; dmgH2 = dimethyl-glyoxime; py = pyridine

Journal Name RSCPublishing

ARTICLE

Graphical Abstract

An energetics and efficiency analysis of a gallium phosphide semiconductor functionalized with molecular hydrogen production catalysts yields insights to designing improved photocathodes.